Sky Radiometer Measurements of Aerosol Optical Properties over Sapporo, Japan

Kazuma AOKI

Graduate School of Environmental Earth Science, Hokkaido University, Sapporo, Japan

and

Yasushi FUJIYOSHI

Institute of Low Temperature Science, Hokkaido University, Sapporo, Japan

(Manuscript received 17 January 2002, in revised form 13 February 2003)

Abstract

Ground-based sky radiometers were used to measure direct solar irradiance and solar aureole radiance for several years at Sapporo, Tsukuba, and Tokyo, Japan. From these measurements, we computed aerosol optical thickness at 0.5 μm, $\tau(0.5)$, and the Ångström exponent, α, and volume size distributions within a column.

The optical thickness at Sapporo increased markedly over a short period of time following Asian dust events, and a forest fire in Siberia. The columnar volume size distributions observed during the Asian dust events showed a peak radius of 2.0–3.0 μm. Backward trajectory analyses suggest that the particles producing this springtime event originated in the Loess Plateau and Gobi Desert, and reached Sapporo via southern China. The columnar size distribution during the forest fire case showed an increase in the density of particles with a peak radius ∼0.2 μm. Trajectory analysis clearly linked the atmospheric changes over Sapporo with a forest fire in Siberia.

The aerosol optical thickness, $\tau(0.5)$, has a clear seasonal cycle at Sapporo, with a vernal maximum and an autumnal minimum. The Ångström exponent, α, has a clear seasonal cycle at both Tokyo and Tsukuba, where early-winter maxima and springtime minima are observed, but at Sapporo the seasonal cycle is weaker, with a summer maximum and a vernal minimum. Aerosols were classified into four types (Types I∼IV) based on $\tau(0.5)$, and α data observed at the three sites. Aerosols with a $\tau(0.5)$ smaller than the total mean of $\tau(0.5)$, but greater than or equal to the total mean of α ($\tau(0.5) < \bar{\tau}(0.5), \alpha \geq \bar{\alpha}$) were classified as Type I; aerosols with $\tau(0.5) \geq \bar{\tau}(0.5)$ and $\alpha \geq \bar{\alpha}$ were Type II; those with $\tau(0.5) < \bar{\tau}(0.5)$ and $\alpha < \bar{\alpha}$ were Type III; and those with $\tau(0.5) \geq \bar{\tau}(0.5)$, $\alpha < \bar{\alpha}$ were Type IV. The most common aerosol type, that is, the background aerosol, was Type I (∼40%) at all three sites. Type-IV aerosols at all three sites showed the same seasonal cycle (spring maximum), suggesting large-scale phenomena such as Asian dust events may contribute to the production and transport of this aerosol type. The behavior of Type-II aerosols differed at the three sites, indicating that local phenomena are important in the production and transport of Type-II aerosols. The emission of manufactured aerosols and subsequent gas-to-particle processes may contribute to Type-II aerosol formation. Type-III aerosols at Sapporo were characterized by a seasonal cycle opposite to that of Type-IV aerosols, suggesting that large particles have different sources and/or transport processes in spring and autumn.

Corresponding author and present affiliation: Kazuma Aoki, Faculty of Education, Toyama Univ., 3190 Gofuku Toyama 930-8555, Japan.
E-mail: kazuma@edu.toyama-u.ac.jp

The atmospheric turbidity retrieved from the sky radiometer is compared, β(SR), at Sapporo with that calculated using direct solar radiation measurements, β(DSR). Both showed the same seasonal cycle, but β(SR) was slightly smaller ($\sim$0.02) than β(DSR).

Sky radiometers can retrieve the optical properties of aerosols under cloudy conditions if there are no clouds around the solar aureole. The seasonal mean of $\tau(0.5)$ (or α) under cloudy conditions was 1.5 to 1.8 (1.1 to 1.2) times larger (smaller) than under clear sky conditions. In other words, the direct effect of aerosols that exist in clear air between clouds cannot be ignored. We call this the hybrid effect of aerosols.

1. Introduction

The effect of aerosols on climate is twofold. Aerosols scatter or absorb shortwave and longwave radiation in the air (the direct effect: e.g., Charlson et al. 1992), and they affect the size distribution of cloud droplets (the indirect effect: e.g., Twomey et al. 1984). Understanding the direct effect of aerosols requires knowledge of the optical properties and temporal and spatial variability of aerosols. The global distributions of Ångström parameters have recently been derived from NOAA/AVHRR data (e.g., Higurashi et al. 2000), and have been simulated in atmospheric general circulation models (AGCMs) (e.g., Takemura et al. 2000), which assume shapes, chemical components, and size distributions of aerosols. Satellite-derived Ångström parameters agree with those derived from ground-based sky radiometers (Nakajima et al. 1999a). However, the global distribution of the optical properties of aerosols is difficult to derive because of strong variability in both time and space. Therefore, long-term monitoring of aerosols from the ground is important and necessary to validate satellite-derived and model-simulated values.

Recent studies have shown that aerosols are transported from East Asia to the North Pacific (e.g., Jaffe et al. 1999). Higurashi et al. (2000) showed that both aerosol optical thickness and the Ångström exponent are large between 40°N and 60°N in April and July. They suggested that a gas-to-particle conversion process is responsible, because there are sources of anthropogenic aerosols in industrial areas. Zhao et al. (2000) and Tanimoto et al. (2000) suggested that Siberian forest fires contribute to the CO concentrations observed in northern Japan (Moshiri and Rishiri, Hokkaido).

Asian dust particles (so-called "yellow sand" in English or Kosa in Japanese) are the typical aerosols transported from the Asian continent to the Pacific Ocean (e.g., Shaw et al. 1980; Uematsu et al. 1983) and North America (e.g., Husar et al. 2001). Researchers have noted the effects of Asian dust events in central and southern Japan (e.g., Arao and Ishizaka 1986; Tanaka et al. 1989; Murayama et al. 2001; Suzuki et al. 2001; Arao and Aoki 2001). These events occur most frequently in spring, with a secondary maximum in autumn (e.g., Nagoya University 1991). The seasonal variation in the amounts of Asian dust particles in northern Japan differs from that in central and southern Japan because of the effects of the summer monsoon (Yamazaki et al. 1999). However, only a few researchers have described Asian dust events in northern Japan (e.g., Murayama et al. 2001).

High latitudes, especially the Arctic and Antarctic, are regions where various materials are deposited. Arctic haze and Arctic summer stratus strongly influence the global radiative heat budget and consequently the global climate. Arctic haze is most common in late winter and early spring (e.g., Atmospheric Environment 1981, 1985, and 1989). Barrie et al. (1988) reported that the transport of anthropogenic aerosols from mid-latitudes to the Arctic occurs mainly in winter. On the other hand, Kawamura et al. (1996) found that soil dust particles are transported from East Asia to high latitudes, including the Arctic, mainly in spring. Further study on the transport mechanism from middle to high latitudes is needed.

The studies noted above underscore the importance of monitoring aerosols. Long-term and seasonal variation must be understood at both low and high latitudes. The Aerosol Robotic Network (AERONET: Holben et al. 1998) and SKYNET (http://atmos.cr.chiba-u.ac.jp/aerosol/skynet/index.html) are ground-based sun- and sky-scanning radiometer networks. Since the sun- and sky-scanning radiometer is a convenient, portable instrument for measuring the

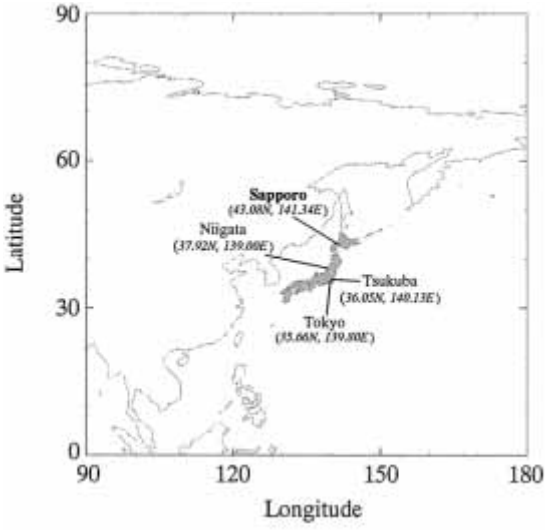

Fig. 1. Location of the observation sites at Sapporo (*43.08 N, 141.34 E*), Niigata (*37.92 N, 139.00 E*), Tsukuba (*36.05 N, 140.13 E*) and Tokyo (*35.66 N, 139.80 E*), Japan.

optical properties of aerosols, the total number of AERONET sites (see http://aeronet.gsfc.nasa.gov:8080/ for site information) has increased rapidly to more than 100. However, most AERONET and SKYNET sites are deployed equatorward of ~60°N. In addition, there was no SKYNET site in Hokkaido, in northern Japan, until July 1997, when a ground-based sky radiometer (see Section 2) began measuring aerosol optical properties at Sapporo (43.08 N, 141.34 E) (Fig. 1). Table 1 shows observation periods at other long-term monitoring sites in Japan (Niigata (37.92 N, 139.00 E), Tokyo (35.66 N, 139.80 E), and Tsukuba (36.05 N, 140.13 E)). This paper presents the results of monitoring the optical properties of aerosols with a sky radiometer over a period of several years. These results will be compared to results from other long-term monitoring sites in central Japan, with special note made of seasonal variation in aerosol optical properties in northern Japan.

2. Instrumentation

The ground-based sky radiometer (POM-01; manufactured by Prede Co., Ltd., Tokyo, Japan) is a convenient, portable instrument that takes measurements only in daytime under clear skies. The radiometer includes a sun- and sky-scanning spectral radiometer, a sun sensor, a sun tracker, a control unit, a rain sensor, and a personal computer (Fig. 2), that is based on auleolemeter (Shiobara et al. 1991). It measures the direct solar irradiance and the solar aureole radiance distributions, and has seven interference filters. In our analysis, we used five wavelengths (0.4, 0.5, 0.675, 0.87, 1.02 μm) to monitor aerosols. The other two wavelengths (0.315 and 0.94 μm) can be used to estimate total ozone and precipitable water (Shiobara et al. 1996), topics beyond the scope of this paper. The instrument has a 1.0° full-angle field of view, and a detector with a dynamic range of 10^7. Detector sensitivity is strongly dependent on temperature, so the detector temperature is kept constant at 30°C. Thirty seconds elapse during the measurement of direct solar irradiance, and the solar aureole radiance distribu-

Table 1. Seasonal mean values of the aerosol optical thickness at 0.5 μm ($\tau(0.5)$) and Ångström exponent (α) in Sapporo, Niigata, Tsukuba and Tokyo, Japan.

Station name	Observation period		$\tau(0.5)$				α			
			DJF	*MAM*	*JJA*	*SON*	*DJF*	*MAM*	*JJA*	*SON*
Sapporo *43.08 N, 141.34 E*	*Jun. 1997 to Aug. 2001*	mean	0.26	0.38	0.28	0.21	1.14	1.09	1.27	1.09
Niigata *37.92 N, 139.00 E*	*Dec. 1994 to Jun. 1997*	mean	0.35	0.44	0.35	0.26	1.10	0.99	1.28	1.12
Tsukuba *36.05 N, 140.13 E*	*Jul. 1995 to Apr. 2000*	mean	0.18	0.37	0.36	0.22	1.21	1.09	1.04	1.15
Tokyo *35.66 N, 139.80 E*	*Nov. 1996 to Nov. 2000*	mean	0.20	0.45	0.37	0.30	1.35	1.09	1.22	1.30

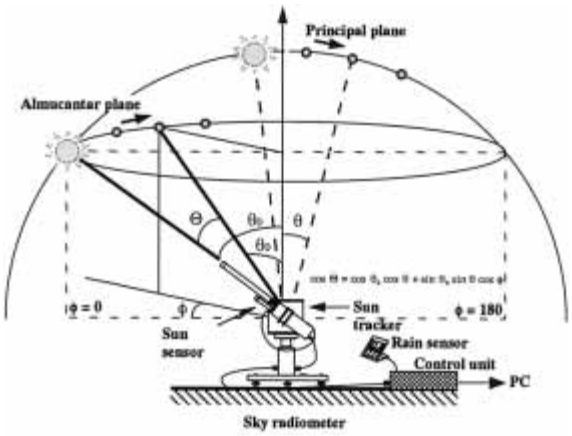

Fig. 2. Geometry of the ground-based sky radiometer system. The sky radiometer includes a sun- and sky-scanning spectral radiometer, a sun sensor, a sun tracker, a control unit, a rain sensor, and a personal computer. Diffuse solar radiation is measured by two different scanning methods depending on the solar zenith angle, θ. The scattering angle Θ is related to θ_0, and to observation angle θ and ϕ. See detail in text.

tion up to 30°. Measurements were made every 10 minutes at Sapporo and every 15 minutes at other sites. The scanning method is described in detail in Tonna et al. (1995). As shown in Fig. 2, diffuse solar radiation is measured by two different scanning methods depending on the solar zenith angle, θ. The almucantar scanning method is selected when $\theta \geq 15°$, and the principal plane scanning method is selected when $\theta < 15°$. The scattering angle Θ is related to θ_0, and to observation angle θ and ϕ as follows:

$$\cos\Theta = \cos\theta_0 \cos\theta + \sin\theta_0 \sin\theta \cos\phi. \quad (1)$$

$\theta = \theta_0$, when almucantar scanning method is used, letting the azimuth angle ϕ vary. $\phi = 0$ when principal plane scanning method is used, letting the zenith angle θ vary.

Direct and diffuse solar radiation are measured. Direct solar radiation $F(\lambda)$ (W m^{-2} μm^{-1}) at each wavelength (λ) is given by

$$F(\lambda) = F_0(\lambda) \exp(-m\tau_t(\lambda)), \quad (2)$$

where $F_0(\lambda)$ is the flux at the top of the atmosphere, m is the optical air mass approximated as $m = 1/\cos\theta_0$ when $m < 5$, and $\tau_t(\lambda)$ is the total optical thickness. The volume size distribution (dV/dlnr (cm^3 cm^{-2})), aerosol optical thickness at λ μm ($\tau(\lambda)$), and the Ångström exponent (α) were computed using the "SkyRad.pack" inversion algorithm (version 2) developed by Nakajima et al. (1996). The aureole intensity $E(\Theta)$ (W m^{-2} μm^{-1}) was determined using the radiative transfer equation (Liou 1980) and is expressed as follows, using almucantar scanning data:

$$E(\Theta) = Fm\Delta\Omega[\omega\tau P(\Theta) + q(\Theta)], \quad (3)$$

where $\Delta\Omega$ is the solid view angle of the instrument, ω is the single scattering albedo, τ is the optical thickness, and $P(\Theta)$ is the total phase function made up of single ($\omega\tau P(\Theta)$) and multiple ($q(\Theta)$) scattering parts. The aureole intensity $E(\Theta)$ is divided by the direct solar radiation intensity F to give the relative intensity $R(\Theta)$:

$$R(\Theta) \equiv \frac{E(\Theta)}{Fm\Delta\Omega} = \omega\tau P(\Theta) + q(\Theta). \quad (4)$$

Since the normalized intensity $R(\Theta)$ is only slightly affected by deterioration of the interference filters, this method is useful for long-term monitoring. $\Delta\Omega$ was determined using the disk-scanning method (Nakajima et al. 1996; Boi et al. 1999), which is based on measurements within a $2° \times 2°$ area around the solar disk with an angle resolution of 0.1°. We assumed a complex refractive index of aerosols as $1.50 - 0.01i$ (Tanaka et al. 1983; Shiobara et al. 1991), and $1.55 - 0.01i$ (Tanaka et al. 1989) for Asian dust events. The differential scattering coefficient was obtained from $R(\Theta)$ data by an iterative regression scheme that includes multiple scattering. A power law size distribution of aerosols is assumed as an initial condition. Although retrieved size of aerosols ranges from 0.02 to 10.0 μm, the details of reliable size range shows Tonna et al. 1995, Nakajima et al. 1996, and Boi et al. 1999.

The inversion procedure is stable even for low optical thickness. Input parameters include the number and value of wavelengths and scattering angles, the surface albedo for each wavelength $A(\lambda)$, the complex refractive index of aerosols, the solid view angle for each wavelength, the minimum and maximum radii of the aerosol particles, and the longitude and

latitude. In this analysis, we used the ground albedo as 0.1 except for winter. In winter we used 0.4, because the ground surface is covered with snow. The difference between retrieved $\tau(0.5)$ (and α) is less than 0.01 (and 0.06). Tonna et al. (1995) concluded that the sky radiometer is quite reliable in the field.

Ångström (1964) discussed the relationship between the size distribution of aerosols and the wavelength dependency of optical thickness. Traditionally, 1.0 μm is used as the reference wavelength for the optical thickness; however, this study uses 0.5 μm, because this wavelength is used by the World Meteorological Organization sun photometer and there are long-term records of the aerosol optical thickness around this wavelength. The Ångström parameters are derived using Ångström's Law (Ångström 1961):

$$\tau(\lambda) = \tau(0.5)\left(\frac{\lambda}{0.5}\right)^{-\alpha}, \quad (5)$$

where $\tau(\lambda)$ is the aerosol optical thickness at λ μm. The Ångström exponent α is used to characterize the wavelength dependency of $\tau(\lambda)$, and to provide information on the aerosol size distribution (e.g., Higurashi et al. 2000). For example, fresh smoke composed mainly of accumulation mode aerosols is characterized by large α (>2.0) (Kaufman et al. 1992). Soil dust aerosols composed mainly of coarse mode aerosols are characterized by small α (0.1∼0.5) (Tanaka et al. 1989).

3. Short-term variation of the Ångström parameters and aerosol size distribution caused by Asian dust events and a forest fire

Before discussing the seasonal and interannual variability in aerosol optical properties, we considered two important events that caused large increases in the optical thickness at Sapporo in a short period of time. These were Asian dust events, and a forest fire.

3.1 Asian dust events

Soil dust particles from the Asian continent commonly increase the atmospheric turbidity in spring, especially in western Japan. The dust particles influence both radiation (e.g., Tegen et al. 1996) and cloud formation (e.g., Isono et al. 1959). Table 1 shows that a large $\tau(0.5)$ with a small α frequently occurs in spring at Sapporo, Tokyo, and Tsukuba. Ohta et al. (1997) suggested that soil particles blown from dry ground after the snow thaws were responsible for the vernal increase in turbidity at Sapporo. However, recent satellite data suggest that the dust particles are transported from the Asian continent to a wider region (e.g., Husar et al. 2001; Tratt et al. 2001) and to higher latitudes (e.g., Kawamura et al. 1996) than previously thought.

A strong Asian dust event was observed on 20–21 April 1998, at Sapporo. This event was monitored using a lidar network, (LINK-J; Lidar Network for *kosa* observation in Japan) (Murayama et al. 2001), sun-photometers (Suzuki et al. 2001) and satellite data (Husar et al. 2001). Numerical simulations were also performed (Uno et al. 2001). Figure 3a shows that $\tau(0.5)$ increased from 0.2 to 1.0, and α decreased from 1.0 to 0.2 between 10:08 and 16:07 JST on 20 April. These temporal changes were similar to those at Nagasaki during an Asian dust event in May 1982 (Tanaka et al. 1989) and to those at other sites in Japan (Tsukuba,

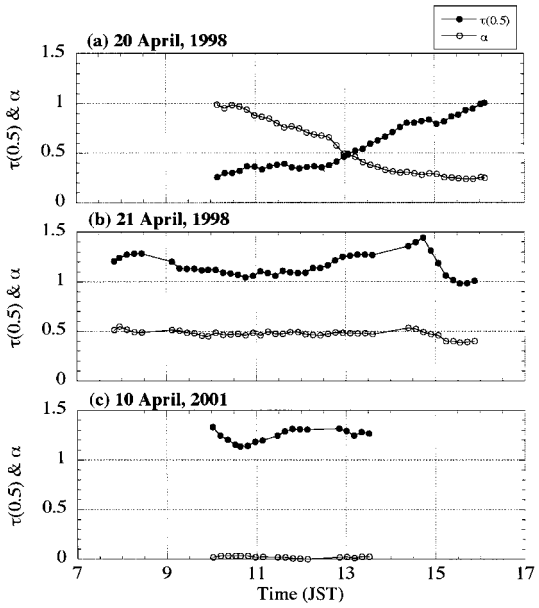

Fig. 3. Time series of the aerosol optical thickness at 0.5 μm ($\tau(0.5)$) (solid circle) and Ångström exponent (α) (open circle) on (a) 20 and (b) 21 April 1998 and (c) 10 April 2001 at Sapporo, Japan.

Tokyo, and Okayama), and Korea (Anmyon Do) (Murayama et al. 2001). On 21 April, $\tau(0.5)$ remained large (~1.2), and α remained small (~0.5) (Fig. 3b).

The second Asian dust event, on 10 April 2001, was exceptionally strong (Fig. 3c), as $\tau(0.5)$ exceeded 1.0 (~1.3), and α was nearly 0. The Japan Meteorological Agency reported that this was the strongest event in 18 years at Sapporo. Indeed, Suzuki et al. (2001) reported the optical properties of Asian dust events in April 1998, and April 1999. Although their observation points in southern Japan were closer to the source region of the dust particles, $\tau(0.5)$ was not as large (<0.84), and α was not as small (0.2–0.5) as in this second event at Sapporo. Tratt et al. (2001) reported that $\tau(0.5)$ ranged from 0.2 to 0.5, and α ranged from 0.2 to 0.7 during a dust event at San Nicolas Island in southern California. The values of $\tau(0.5)$ and α were also less extreme than those of the second Sapporo event.

Figure 4 shows the columnar volume size distributions of Asian dust events at 10:08 (C1), and 16:07 JST (C2) on 20 April 1998, at 8:17 JST (C3) on 21 April 1998, and at 10:10 (C4) on 10 April 2001. The size distributions have peaks at radius 2.0–3.0 μm, similar to distributions observed in Korea and western Japan (Tanaka et al. 1989; Murayama et al. 2001). Large particles are lost more rapidly than small particles during transport, and the radius at the peak value in the volume size distribution at Sapporo is much smaller than that of particles (~5.0 μm) observed at the source of the dust particles (Gobi Desert) (Husar et al. 2001). However, the volume size distributions on 20 and 21 April showed an interesting temporal evolution (Fig. 4). Aerosols with radii larger than 0.5 μm increased from C1 to C2. Aerosols with radii smaller than 0.5 μm increased from C2 to C3. Larger particles arrived at Sapporo before smaller particles! A lidar network (such as LINK-J) and wind profilers are necessary to monitor the detailed vertical distribution of particles and to investigate further the transport mechanism. Sky radiometers, however, can yield useful information, especially about the short-term variation of the size distribution.

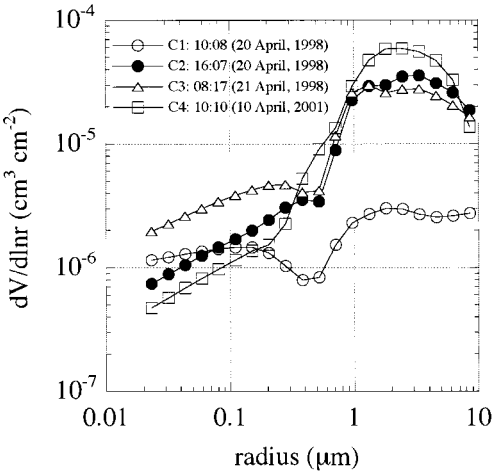

Fig. 4. Typical columnar volume size distribution (dV/dlnr (cm^3 cm^{-2})) of the Asian dust events observed at 10:08 JST (C1) and 16:07 JST (C2) on 20 April 1998, 8:17 JST (C3) on 21 April 1998 and at 10:10 (C4) on 10 April 2001.

We studied the spring event (21 April 1998) using backward trajectories computed with the trajectory model of Yamazaki et al. (1999). The model has a grid size of $2.5^\circ \times 2.5^\circ$, and 15 vertical layers. The backward trajectories originated as 1331 particles ($11 \times 11 \times 11$) in a $1.0^\circ \times 1.0^\circ$-grid box around Sapporo. Initial height of particles ranged from near surface to 500 hPa at each grid point. The particles were advected backward in time using 3-D winds from the ECMWF objective analysis. The wind at each individual particle grid point was interpolated from the surrounding ($2.5^\circ \times 2.5^\circ$) grid points. Horizontal and temporal interpolations were linear. A cubic spline interpolation was used in the vertical. The time step was 20 minutes. Figure 5 shows the results of 7-day backward trajectories, and plots the vertically integrated concentration of the simulated dust particles. The analysis suggests that the particles of the spring event originated over the Loess Plateau and the Gobi Desert, and reached Sapporo via southern China. This agrees with the analysis of Murayama et al. (2001).

3.2 Siberian forest fires

Tanimoto et al. (2000) found that Siberian forest fires significantly increased carbon monoxide (CO) in summer and early autumn in

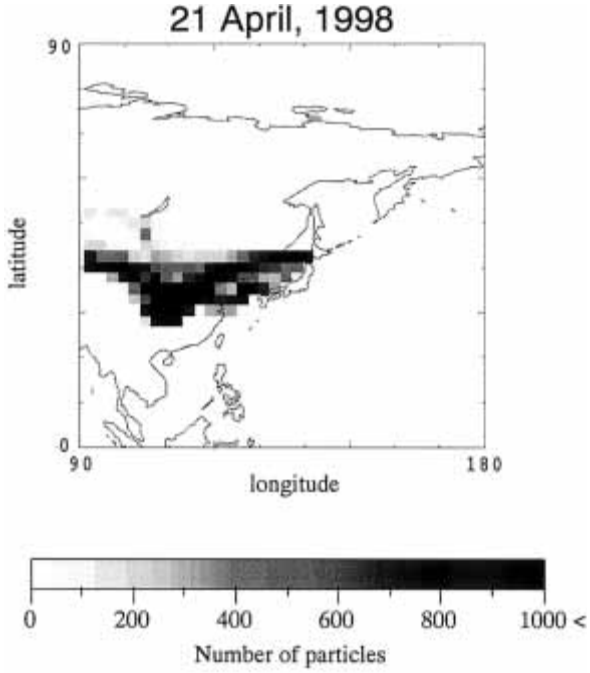

Fig. 5. The results of the 7-day backward trajectory analysis started from Sapporo at 21 April 1998. See detail of the calculation procedure in text.

1998 at Rishiri Island (45.07 N, 141.12 E), Hokkaido, Japan. The aerosol optical thickness at 0.5 μm ($\tau(0.5)$) and Ångström exponent α are usually about 0.3 and 1.3 in summer at Sapporo, respectively. However, exceptionally large $\tau(0.5)$ (~0.4) and α (~1.7) were observed on 21 August 1998 (Fig. 6). These values exceed those accompanied an Indonesian forest fire event (Nakajima et al. 1999b), and are similar to those observed during biomass burning at Mongu, Zambia (Holben et al. 2001).

Figure 7 shows volume size distributions for the August 1998 case. The forest fire case

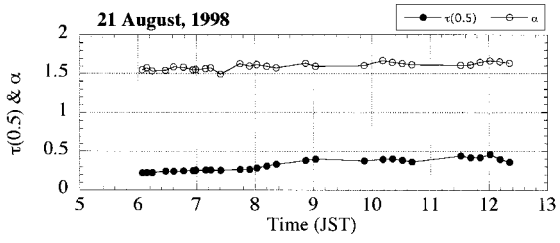

Fig. 7. Same as in Fig. 4, but on 21 August 1998.

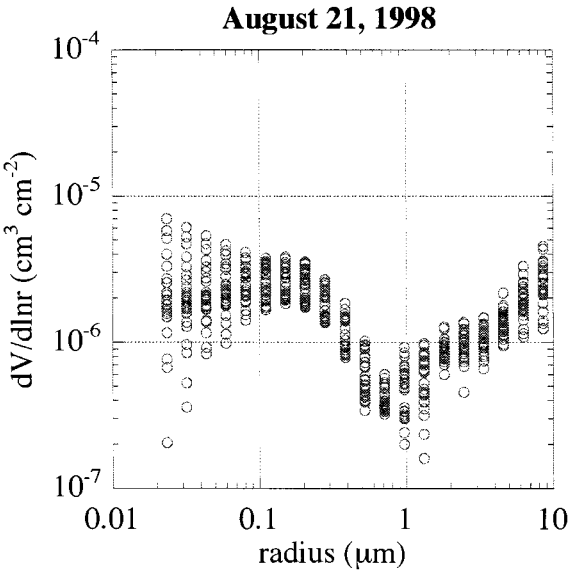

Fig. 6. Same as in Fig. 3, but on 21 August 1998.

was characterized by an increase in the number of small particles with a peak radius ~0.2 μm, which is similar to the result reported by Holben et al. (2001). The trajectory analysis (Fig. 8) shows that the particles originated near a Siberian forest fire (see http://ptah.gvm.sai.jrc.it/wfw/). Since this is only one case study, however, it is not clear whether forest fires routinely influence the seasonal variation of aerosol optical properties at Sapporo. However, this Siberian forest fire did affect aerosol optical properties over northern Japan, and warrants further investigation.

4. Seasonal variation of Ångström parameters and aerosol size distribution at Sapporo

Long-term monitoring of aerosol optical properties at Sapporo, Hokkaido, the northernmost island of Japan, began in July 1997. Local sources of pollutants at Sapporo are mainly emissions from automobiles, and from oil combustion for domestic heating. Figure 9 shows the temporal evolution of the monthly mean $\tau(0.5)$, and α from July 1997 to August 2001. Cloud contamination and other factors limited the analysis to only 30% of observed data. The monthly mean value (solid circle) of $\tau(0.5)$ shows the same seasonal cycle for four years,

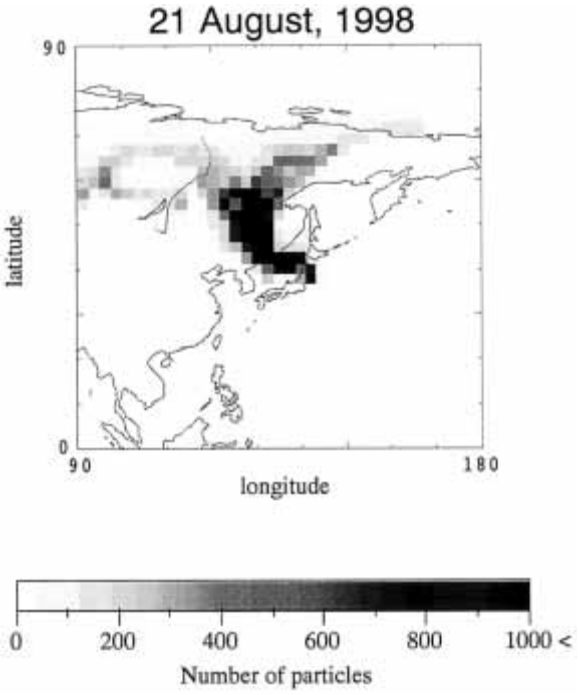

Fig. 8. Same as in Fig. 5, but on 21 August 1998.

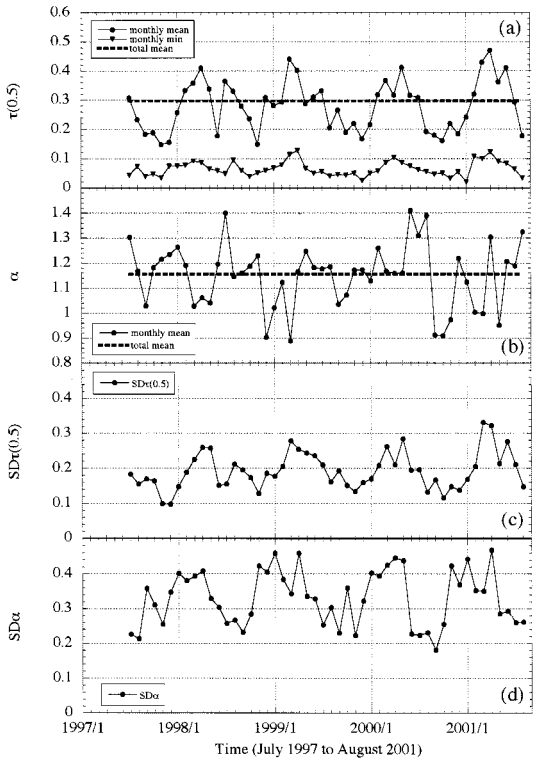

Fig. 9. Temporal variation of the aerosol optical thickness at 0.5 μm ($\tau(0.5)$) and Ångström exponent (α), averaged monthly for the period from July 1997 to August 2001 in Sapporo. (a) and (b); The solid and triangle indicates the monthly mean and minimum values of $\tau(0.5)$, respectively. The total mean (broken line) of $\tau(0.5)$ and α is 0.30 and 1.16, respectively. (c) and (d); standard deviations of $\tau(0.5)$ and α.

with maxima and minima appearing in spring and autumn, respectively (Fig. 9a). Peak values are similar for the four years (minimum $\sim$ 0.15 and maximum $\sim$ 0.45). The total means (broken line) of $\tau(0.5)$ and α are 0.30 and 1.16, respectively. The minimum value of $\tau(0.5)$ in each month (solid triangle in Fig. 9a) is small (less than 0.1), and it shows the same seasonal cycle as the monthly mean values. The standard deviation of $\tau(0.5)$ (SD$\tau(0.5)$ in Fig. 9c) shows variation similar to the monthly mean $\tau(0.5)$. Figure 10 shows that the monthly mean $\tau(0.5)$ is large (or small) when SD$\tau(0.5)$ is large (or small). Although optical thickness is affected by size distribution and number density of aerosols, total number of aerosols is suggested to have a clear seasonal cycle, peaking in spring, as will be shown later.

The values of $\tau(0.5)$ were exceptionally low in June of 1998, compared with other years. Figure 11 shows that the number of aerosols, especially accumulation mode particles, in June of 1998 was much smaller than in other Junes. Precipitation in June of 1998 was 1.5 to 2 times the value for other Junes at Sapporo, suggesting that scavenging of aerosol particles by cloud droplets and precipitation particles might be responsible for the low $\tau(0.5)$. A decrease in $\tau(0.5)$ was also noted in the rainy season (July) at Tsukuba (Takemura et al. 2001).

In contrast to $\tau(0.5)$, monthly mean plots of α show only weak seasonal changes (Fig. 9b). Since α is critically controlled by the size distribution of aerosols, this suggests that the aerosol size distribution does not follow a seasonal cycle. Except for 1999, however, α is relatively small in spring and large in summer, consistent with results from Shiobara et al. (1991), who showed that coarse particle mode aerosols dominate in spring, and accumulation

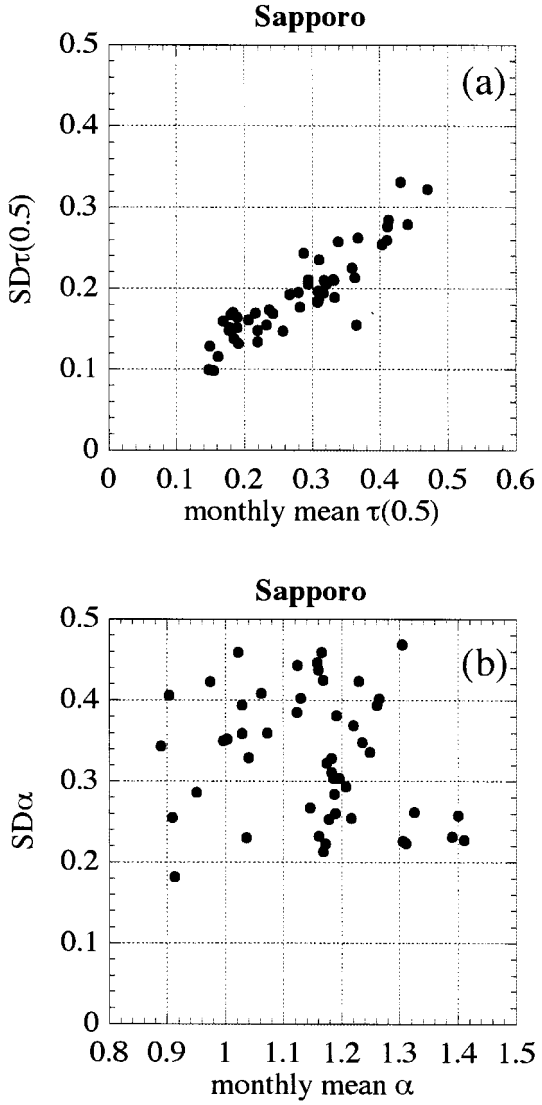

Fig. 10. The relationship between the monthly mean $\tau(0.5)$, α and standard deviation SD$\tau(0.5)$, SDα at Sapporo, Japan.

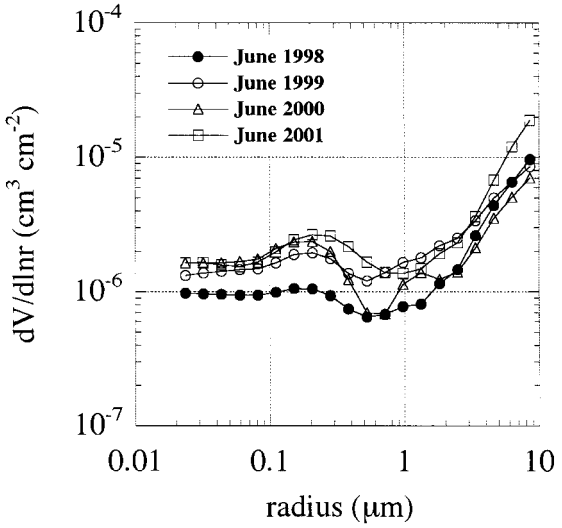

Fig. 11. The monthly averaged volume size distribution in June from 1998 to 2001 at Sapporo.

mode aerosols dominate in summer. Summer 1999 values of α were not large compared to the three other years, and the α value most commonly observed in summer 1999 was smaller than in the other three years (not shown). This suggests that larger particles were more common in summer 1999 for reasons that are not yet clear. α does not correlate with its standard deviation (SDα), as shown in Figs. 9d and 10b, indicating that a large SDα does not necessarily mean the predominance of large or small aerosols. On the other hand, SDα clearly shows a seasonal cycle (Fig. 9d). SDα increases from autumn to spring and decreases from spring to autumn, out of phase with both $\tau(0.5)$ and SD$\tau(0.5)$. This suggests that the temporal change in the aerosol size distribution is largest in spring and smallest in autumn.

All data (*21,797*) are plotted in the scatter diagram of $\tau(0.5)$ and α (Fig. 12). Open circles with error bars mean the averaged $\tau(0.5)$ for ranges of α (0–0.5, 0.5–1.0, 1.0–1.5, and 1.5–2.0). On average, α decreases with increasing $\tau(0.5)$, and the variance of $\tau(0.5)$ decreases with increasing α. Therefore, small particles are not responsible for large optical thickness. By contrast, the predominance of large particles does not necessarily lead to large optical thickness, although extremely large optical thickness occur only when α is very small. Aerosols in spring (MAM: March–May) are characterized by frequent occurrences of small α (<0.5) compared to other seasons. The $\tau(0.5)$ value in autumn (SON: September–November) is small regardless of the value of α. Summer (JJA: June–August) aerosols are different from other seasons as large α (>1.0) aerosols are common, and the variance SDα is small. Figures 12b and 12c indicate that the large SDα in winter (DJF: December–February) and spring (MAM) is due

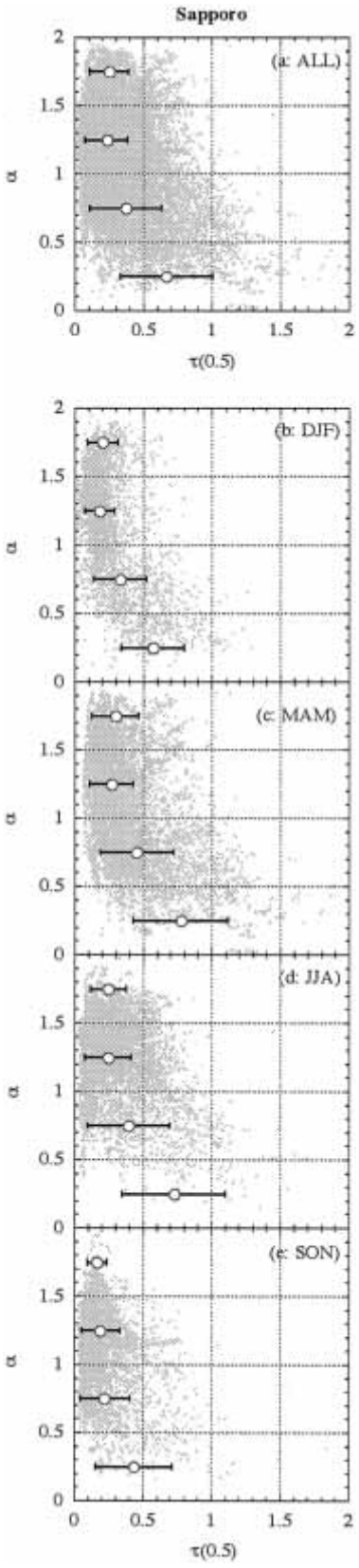

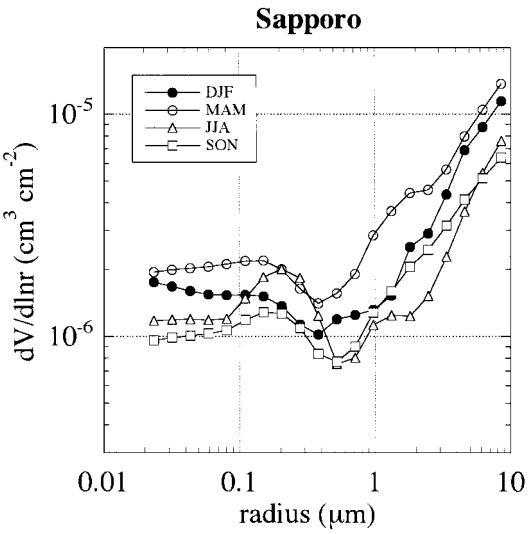

Fig. 13. Seasonal mean values of the volume size distribution (dV/dlnr (cm^3 cm^{-2})) in the respective season at same period in Fig. 12.

to the increased presence of aerosols with small α (<0.5).

The seasonal cycle of Ångström parameters at Sapporo is governed by the increased presence of aerosols with small α (<0.5) in spring, and large α (>1.0) in summer. Large particles become more common from autumn to spring and less common from spring to autumn, and small particles are very common in summer. Figure 13 shows seasonally averaged volume size distributions (dV/dlnr) and shows that the number of aerosols in MAM exceeds that of other seasons. The number of coarse mode particles is especially large. The mean number in DJF is smaller than in MAM, but larger than in

Fig. 12. Scatter plots of aerosol optical thickness at 0.5 μm $\tau(0.5)$ and Ångström exponent α in the respective season (All: all season data, DJF: December–February, MAM: March–May, JJA: June–August, SON: September–November) from July 1997 to August 2001 at Sapporo, Japan. Open circles with error bars mean the averaged $\tau(0.5)$ for ranges of α (0–0.5, 0.5–1.0, 1.0–1.5, and 1.5–2.0).

SON and JJA. Figure 13 also shows an increase in the number of accumulation mode particles (around 0.2 μm) in summer, consistent with observations at Sendai (Shiobara et al. 1991), and Tsukuba (Hayasaka et al. 1998).

The results in Section 3 indicate that Asian dust particles are actually transported to Sapporo (i.e., northern Japan). Considering synoptic conditions and the atmospheric circulation, Yamazaki et al. (1999) concluded that Asian dust particles transported to northern Japan in autumn might have different source region from those in spring. This could explain why the seasonal cycle of optical thickness at Sapporo is not clearer than at Tsukuba or Tokyo (western and southern Japan).

5. Comparison with other monitoring sites

Two sites in Japan (Tsukuba; 36.05 N, 140.13 E and Tokyo; 35.66 N, 139.80 E) (Fig. 1) have data from long-term monitoring. Tokyo is a typical metropolitan urban area on the Pacific Ocean. Tsukuba is more rural, and is approximately 60 km northeast of Tokyo. Figure 14a shows that the monthly mean $\tau(0.5)$ at both sites has the same seasonal cycle as Sapporo. A maximum occurs in spring, and a minimum occurs in autumn and winter. However, the amplitude of the seasonal cycle at Tokyo is larger than at Sapporo. The spring maximum of optical thickness in southern and central Japan is caused by Asian dust events (e.g., Tanaka et al. 1989; Murayama et al. 2001). In contrast to Sapporo, α (Fig. 14b) also has a clear seasonal cycle at both sites, with a maximum in late autumn to early winter and a minimum in spring. Mizuno and Kondo (1992) reported that air pollution measured by suspended particles (SP) and NO_x increased from late autumn to early winter on the Kanto Plain, which includes Tsukuba and Tokyo. The maximum value of $\tau(0.5)$ (or α) is decreasing (or increasing) year by year at Tsukuba; this long-term trend is not recognized at Sapporo. This suggests that Asian dust events in spring are rarer and that aerosol size in autumn is smaller, but the true reason behind the trend is not yet clear. Takemura et al. (2001) predicts that black carbon and sulfate aerosol values over Japan in 2050 will be two to three times as large as in 2000. Long-term monitoring of aerosol optical properties will confirm the truth behind the trends.

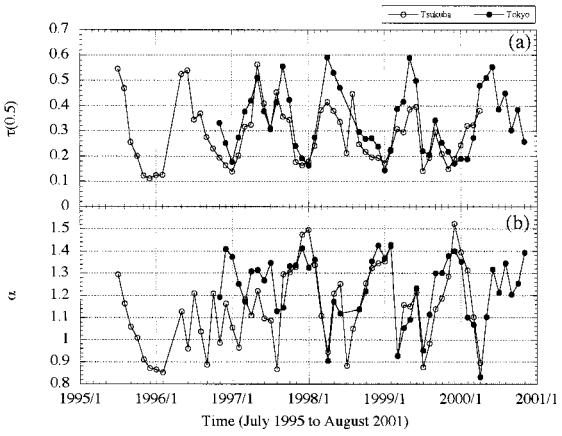

Fig. 14. Temporal variation of the aerosol optical thickness at 0.5 μm ($\tau(0.5)$) and Ångström exponent (α), averaged monthly at Tsukuba and Tokyo.

Figure 15 includes all data and monthly mean $\tau(0.5)$ and α, so that differences between the three sites are clear. The monthly mean $\tau(0.5)$ and α are largest at Tokyo and smallest at Sapporo. $\tau(0.5)$ shows a vernal maximum at all three sites. A minimum occurs in July at Tsukuba and Tokyo, but not at Sapporo. The monthly mean α reaches a maximum in summer at Sapporo, but in winter at Tsukuba and Tokyo. The scatter diagrams of $\tau(0.5)$ and α (Fig. 16) reveal differences in aerosol optical properties between Sapporo, Tokyo, and Tsukuba (and Niigata). Aerosols at Tokyo and Tsukuba have nearly the same optical properties and show similar seasonal changes. The scatter diagram for summer at Sapporo (Fig. 12) is similar to that at Tokyo and Tsukuba, but is very different for autumn and winter. Aerosols with small α and large $\tau(0.5)$ appear more frequently in autumn and winter at Sapporo than at Tokyo and Tsukuba. Aerosols at Niigata have the same tendency as those at Sapporo in autumn and winter, and it is tempting to speculate that the reason is ejection of sea salt from the Sea of Japan.

Many aerosols contain chemically distinct species, such as sulfates, organics, black carbon, dust, sea salt, or mixtures of these materials. The optical properties of aerosols depend

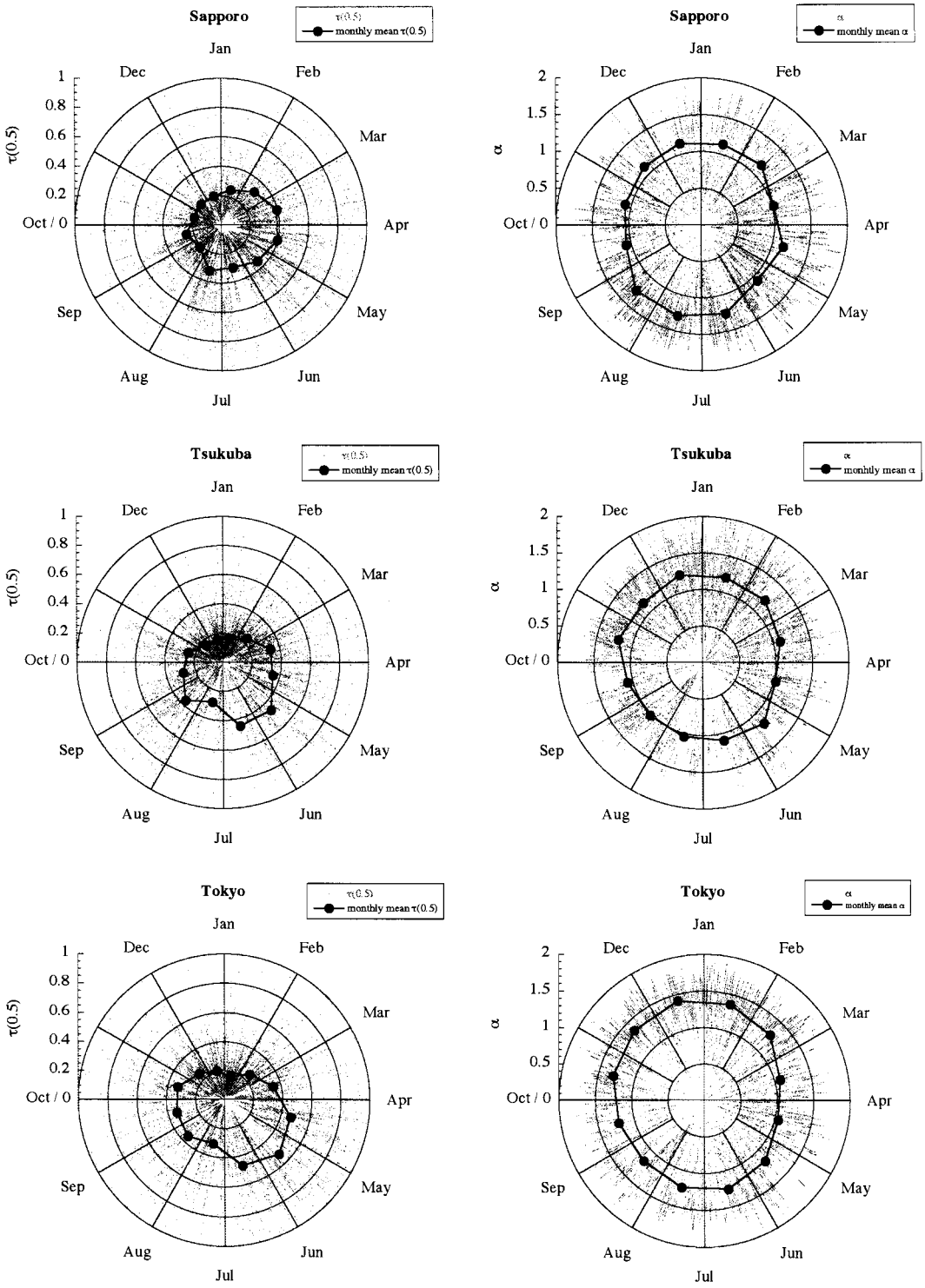

Fig. 15. The seasonal variation of all data (dot) and monthly mean values of $\tau(0.5)$ and α (solid circle) at Sapporo, Tsukuba and Tokyo sites.

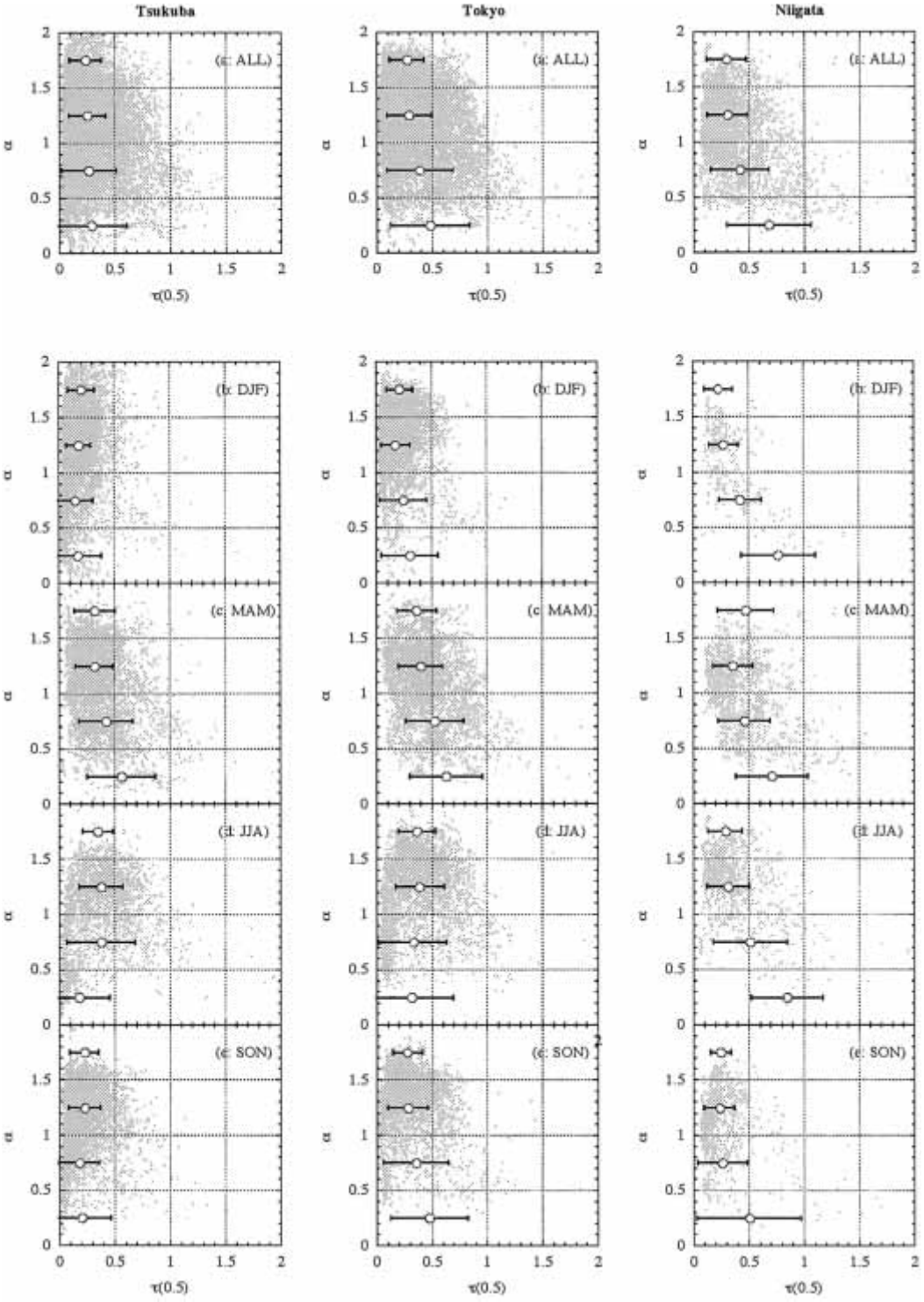

Fig. 16. Same as in Fig. 12, but in Tsukuba, Tokyo and Niigata sites.

Table 2. Number and pecent ratios for each types at three sites.

	Sapporo		*Tsukuba*		*Tokyo*		*Total*	
Type-I	8335	*38.2%*	6958	*35.6%*	7134	*38.6%*	22427	*37.4%*
Type-II	3104	*14.2%*	3103	*15.8%*	4965	*26.8%*	11172	*18.7%*
Type-III	5225	*24.0%*	6201	*31.7%*	3043	*16.5%*	14469	*24.2%*
Type-IV	5133	*23.6%*	3302	*16.9%*	3344	*18.1%*	11779	*19.7%*
Total	21797		19564		18486		59847	

on their chemical makeup. For example, pure sulfate aerosols primarily scatter solar radiation (non-absorbing aerosols), but carbonaceous aerosols (black carbon and organics) scatter and absorb solar radiation (absorbing aerosols). Therefore, it is important to identify the type of aerosol. A new algorithm that can retrieve the aerosol complex refractive index, and the non-sphericity effect in the phase function is being developed (T. Nakajima (CCSR, Univ. Tokyo), private communication), but is not yet available. Instead, we classified aerosols into four types (Types I∼IV) based on all $\tau(0.5)$ and α data observed at the three sites as follows (see also Table 2). Total means of $\tau(0.5)$ and α at the three sites were $\bar{\tau}(0.5) = 0.29$ and $\bar{\alpha} = 1.18$, respectively. We defined Type-I aerosols as those having $\tau(0.5)$ smaller than the total mean of $\tau(0.5)$, and α larger than the total mean of α ($\tau(0.5) < \bar{\tau}(0.5), \alpha \geq \bar{\alpha}$); i.e., relatively smaller particles with small optical thickness. Type-II aerosols are characterized by a $\tau(0.5)$ larger than the total mean $\tau(0.5)$, and an α larger than the total mean α ($\tau(0.5) \geq \bar{\tau}(0.5)$, $\alpha \geq \bar{\alpha}$); i.e., relatively small particles with large optical thickness. Type-III aerosols have a $\tau(0.5)$ smaller than the total mean $\tau(0.5)$, and an α smaller than the total mean α ($\tau(0.5) < \bar{\tau}(0.5), \alpha < \bar{\alpha}$); i.e., relatively large particles with small optical thickness. Type-IV aerosols have a $\tau(0.5)$ larger than the total mean $\tau(0.5)$, and an α smaller than the total mean α ($\tau(0.5) \geq \bar{\tau}(0.5), \alpha < \bar{\alpha}$); i.e., relatively large particles with large optical thickness. Note that this type classification does not necessarily correspond to the classification of species of individual aerosols. Instead, these types are useful for characterizing the atmospheric conditions. We would like to emphasize that it would be impossible to calculate the total means of $\tau(0.5)$ and α, and to use these values as a standard to classify the atmospheric conditions at various sites in Japan without conducting multi-year observations at different sites.

Figures 17, 18, and 19 show how frequently the four types of aerosols appear at Sapporo, Tsukuba, and Tokyo, respectively. Type-I aerosols are more common than any other type at all sites, appearing ∼40% of the time. This suggests that Type-I aerosols are the background aerosols at all three sites in Japan. In other words, the basic atmosphere in Japan contains relatively small particles with small optical thickness. Type-I aerosols are common at Sapporo in both summer and winter, and they are far more common than average in the summer. In contrast, Type-I aerosols are common in winter, but rare in summer at Tsukuba and Tokyo. The atmosphere is very clean in summer at Sapporo, but not at Tokyo or Tsukuba.

Type-IV aerosols are most common in April or May at all three sites. Large particles with high optical thickness are most likely to be found in spring at the three sites, during the period corresponding to *kosa* events. Type-IV aerosols are more common in Sapporo in winter than at Tokyo and Tsukuba, as discussed in Sections 3 and 4.

The seasonal change in Type-III aerosols (larger particles with small optical thickness) at Sapporo is of opposite phase to the seasonal change of Type-IV aerosols there. Type-III aerosols appear infrequently at Tokyo compared to other types. Type-III aerosols are common at Tsukuba, especially in autumn and winter. Type-II aerosols (smaller particles with large optical thickness) appear more frequently at Tokyo than at the other two sites in all seasons. They are especially common in Tokyo in late spring to early autumn. Type-II aerosols

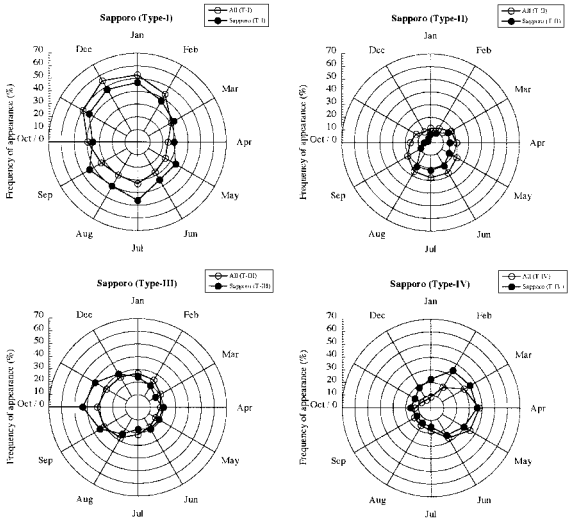

Fig. 17.

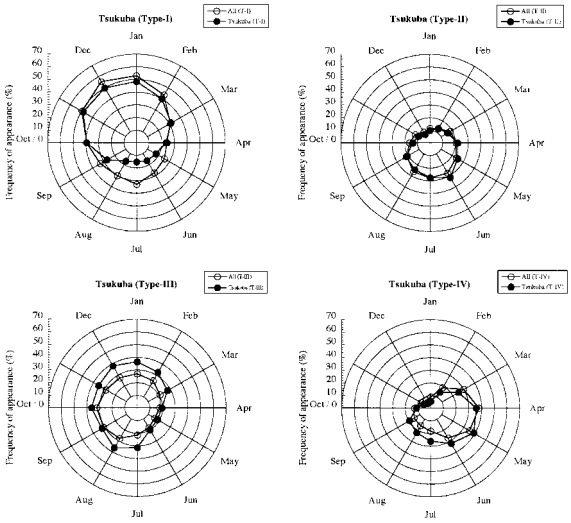

Fig. 18.

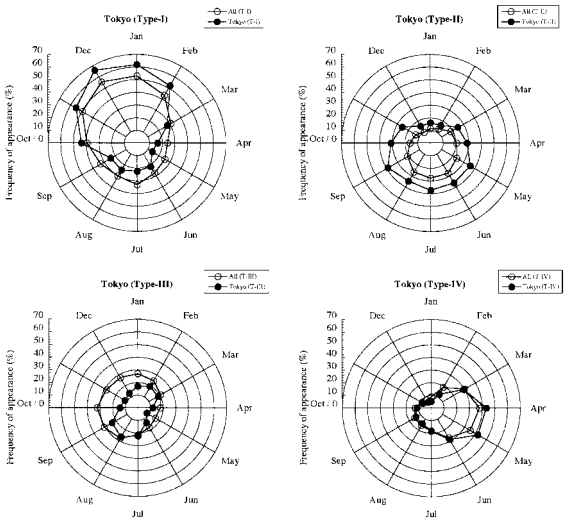

Fig. 19.

Fig. 17. Frequency of appearance $\tau(0.5)$ and α for each types (Type I to Type IV) in Sapporo (solid circle). Open circle is frequency of occurrences of total mean $\tau(0.5)$ and α at the three observation sites. Type I (T-I) is less than total mean of $\tau(0.5)$ and greater than or equal to total mean of α. Type II (T-II) is greater than or equal to total of $\tau(0.5)$ and greater than or equal to total mean of α. Type III (T-III) is less than total mean of $\tau(0.5)$ and less than total mean of α. Type IV (T-IV) is greater than or equal to total mean of $\tau(0.5)$ and less than total mean of α.

Fig. 18. Same as in Fig. 17, but in Tsukuba.

Fig. 19. Same as in Fig. 17, but in Tokyo.

at Sapporo show the same seasonal cycle as Tokyo, but the frequency of appearance is much smaller.

In summary, Type-I aerosols are the background aerosol at all three sites. Type-IV aerosols have the same seasonal cycle (spring maximum) at all three sites, indicating that large-scale phenomena, such as "Kosa" events, contribute to the production and transport of this aerosol type. The appearance of Type-II aerosols differs between the three sites, indicating that local phenomena dominate the production and transport of this aerosol type. Since Type-II aerosols are most common in summer in Tokyo, anthropogenic aerosol emission and subsequent gas-to-particle processes are likely candidates for the formation of this aerosol type. Type-III aerosols show a seasonal

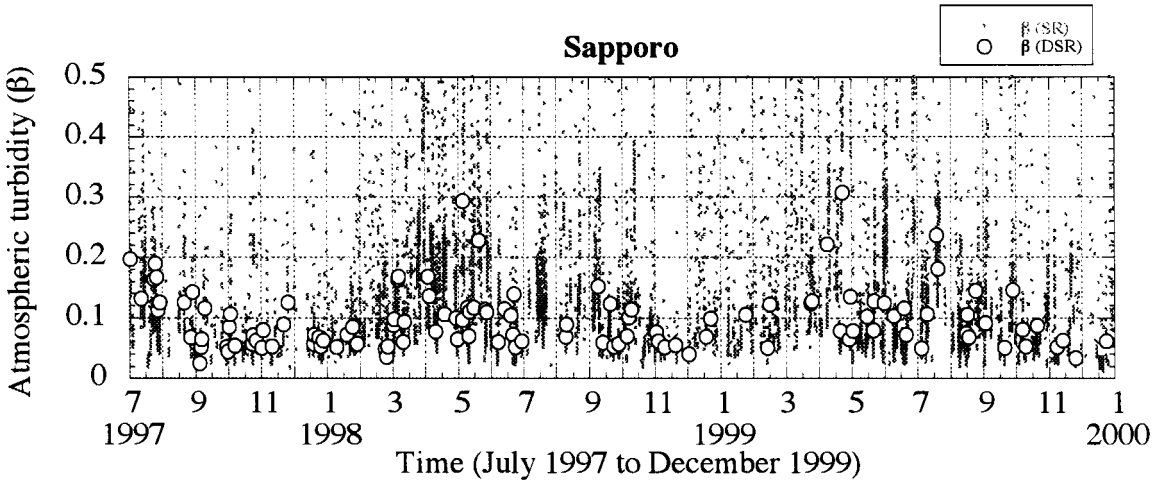

Fig. 20. Time series of the atmospheric turbidity β retrieved from sky radiometer (β(SR)) (dot) in comparison with that obtained from direct solar radiation measurements (β(DSR)) (open circle) from July 1997 to December 1999 at Sapporo.

cycle opposite to that of Type IV at Sapporo, suggesting a difference in the sources and/or transport of larger particles between spring and autumn. To confirm this suggestion, further field and modeling studies would be necessary. Table 1 summarizes the seasonal mean values of Ångström parameters at Sapporo, Niigata, Tsukuba, and Tokyo, locations where measurements have been made for between two and five years.

6. Long-term and seasonal variation in atmospheric turbidity

By comparing our results with past studies, we can learn more about the long-term variation of the optical thickness of aerosols. Direct comparison of our results with past studies is not possible. Instead, we calculated the atmospheric turbidity coefficient β ($=\tau(0.5) \times 0.5^{\alpha}$), which has been observed at several sites in Japan since the 1930s (Yamamoto et al. 1968; Yamamoto et al. 1971; Arao 1974). Combining these results with those of Arao and Yamamoto (1981), Ohta et al. (1997) determined the long-term variation of β since the 1950s at five sites in Japan (Nemuro, Sapporo, Shionomisaki, Tosashimizu, and Ishigakijima). They concluded that β in rural areas of Japan (Nemuro, Shionomisaki, and Tobishima) increased by 0.03 to 0.06 over these 35 years. Greater emissions of pollutants in Japan, and increased long-range transport of pollutants from China could have caused this increase. Ohta et al. (1997) also reported that β at Sapporo increased in the late 1960s due to increased coal combustion for domestic heating, and decreased in the 1970s as coal was replaced by kerosene. After the mid 1970s, the only increase was short-term increases due to the volcanic eruptions of El Chichon in 1982, and Pinatubo in 1991.

Figure 20 shows atmospheric turbidity, β, from July 1997 to December 1999 at Sapporo, retrieved from a sky radiometer (β(SR)) (dots) and calculated from direct solar radiation measurements (β(DSR)) (open circles) (S. Ohta (Hokkaido Univ.), private communication). Both turbidity measurements show the same seasonal cycle. However, the amplitude and number of β(SR) is greater than that of β(DSR). Direct solar radiation can be measured only under clear sky conditions. Therefore, few β(DSR) measurements can be made. β(SR) is compared with β(DSR) in Figure 21, which shows that β(SR) is slightly smaller ($\sim$0.02) than β(DSR). The relationship between β(SR) and β(DSR) differs during DJF from other times in the year. A change in surface albedo caused by snowfall as noted in section 2 could explain this difference. Further monitoring of the aerosol optical properties with a sky radiometer will confirm the trends and help explain the reason for the differences.

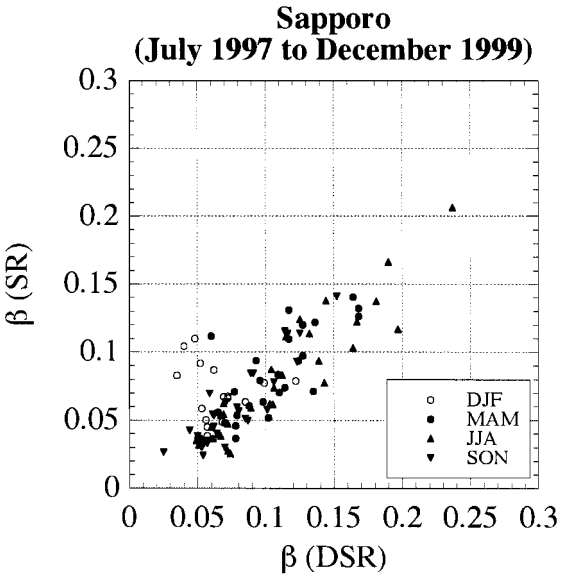

Fig. 21. A comparison of the atmospheric turbidity for common times during the same period in Fig. 20 at Sapporo in the respective season.

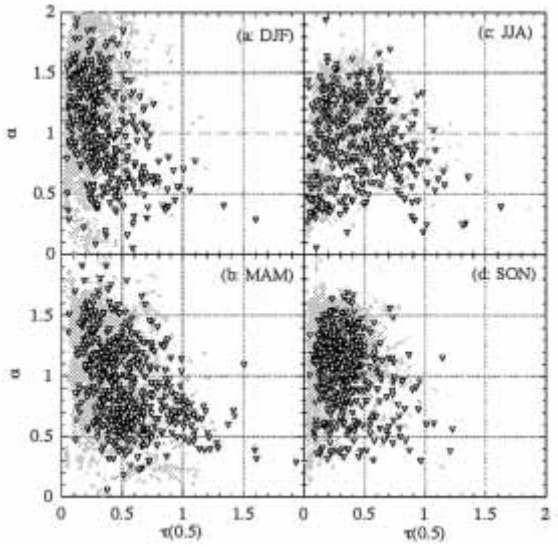

Fig. 22. Scatter plots of aerosol optical thickness at 0.5 μm $\tau(0.5)$ and Ångström exponent α in the respective season from June 1996 to April 2000 at Tsukuba, Japan. Open circles denote data measured under clear skies, whereas open triangles represent data measured under cloudy conditions.

7. Effect of aerosols between clouds

Aerosol and clouds have the dominant effect on the earth radiation budget. A sky radiometer system can measure columnar optical property of aerosol (Nakajima et al. 1996). However, quantitative retrieval of vertical profiles and cloud contamination from the measured columnar optical property is impossible.

Cloud screening can improve the accuracy of retrieved aerosol optical properties from ground-based (Smirnov et al. 2000), and satellite (Higurashi et al. 2000) measurements. At AERONET sites, the screening algorithm of Smirnov et al. (2000) eliminates 20 to 50% of the initial data. We eliminated 30 to 70% of the initial data because of cloud conditions and other factors. The sky radiometer, however, measures optical properties of aerosols under partly cloudy conditions if there are no clouds within 30° of the solar aureole radiation distribution. Since the relative humidity is high under cloudy conditions, the optical properties of aerosols that exist in between clouds would be changed. To study the properties, we compare the optical properties of aerosols measured under partly cloudy conditions with those measured under fully fine weather conditions.

We analyzed data measured from June 1996 to April 2000 to quantify the optical properties of aerosols between clouds. Data include simultaneous measurements from a lidar and a sky radiometer at the National Institute for Environmental Studies (NIES) at Tsukuba. The measurements were made in daytime every fifteen minutes. Vertical profiles of backscattering coefficients of aerosol and cloud were obtained using the vertically pointing Mie lidar (a pulsed Nd:YAG laser at 0.532 μm) up to 15 km. Its vertical resolution was 7.5 m until March of 1999, and 6.0 m after April of 1999. Following the threshold method presented by Sassen and Cho (1992), we classified the sky conditions (weather) above Tsukuba into three categories, i.e., clear (clear sky condition, and the lidar signal is less than the threshold), cloudy (cloudy sky condition, and the lidar detected the cloud base for a single profile) and other (rain and no data) conditions.

Clouds were often detected during the observation period. The relationship between α and $\tau(0.5)$ is shown in Fig. 22. Open circles de-

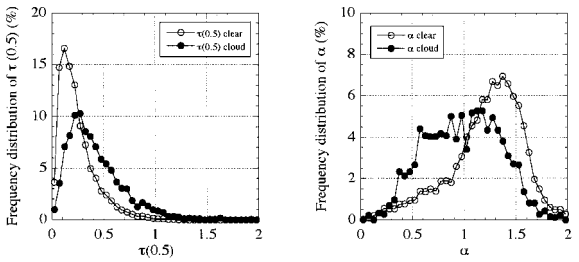

Fig. 23. The relationship between clear skies and cloudy condition of frequency distribution of $\tau(0.5)$ and α. Open circles denote data measured under clear skies, whereas open triangles represent data measured under cloudy conditions.

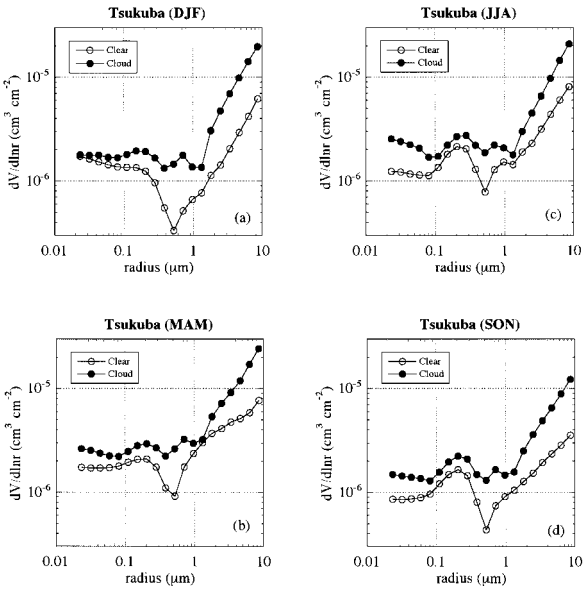

Fig. 24. The relationship between clear skies and cloudy condition of seasonal means of the volume size distribution. Open circles show in the clear sky, while solid circles correspond to the data in the cloud condition.

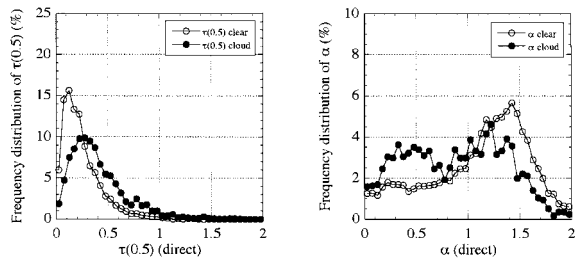

Fig. 25. Same as in Fig. 23, but on retrieved from direct solar radiation.

note data measured under clear skies, whereas open triangles represent data measured under cloudy conditions. The values of $\tau(0.5)$ (or α) measured under cloudy condition are slightly larger (or smaller) than those measured under clear conditions in all seasons. The frequency distributions of the Ångström parameters are summarized in Fig. 23. The seasonal mean of $\tau(0.5)$ (or α) measured under cloudy conditions is 1.5 to 1.8 (or 1.1 to 1.2) times greater (or smaller) than that measured under clear skies. The direct effect of aerosols that exist between clouds cannot be ignored. We call this effect the hybrid effect of aerosols. Figure 24 shows seasonal means of the volume size distribution measured under clear (open circle) and cloudy (closed circle) skies. The number of aerosols measured under cloudy skies is greater than under clear skies in all seasons. The number of aerosols with radius greater than 0.5 μm in radius is notably large.

To check whether scattering by clouds contaminates the calculation using aureole, we calculated $\tau(0.5)$ and α using direct solar radiation (Fig. 25). The appearance frequencies of $\tau(0.5)$ and α in Fig. 25 are similar to those in Fig. 23. Therefore, the hybrid effect of aerosols is real.

8. Conclusions

Measurements of the optical properties of aerosols from sky radiometers over several years at Sapporo, Tokyo, and Tsukuba yielded the following conclusions:

1. The aerosol optical thickness $\tau(0.5)$ shows a clear seasonal cycle (vernal maximum, autumnal minimum) at Sapporo. At Tokyo and Tsukuba, $\tau(0.5)$ shows a seasonal cycle similar to that at Sapporo, but with a winter minimum. Although the Ångström exponent α shows a clear seasonal cycle at Tokyo and Tsukuba (maximum in early winter and minimum in spring), it shows a weak seasonal cycle (maximum in summer and minimum in spring) at Sapporo.
2. We classified aerosols into four types (Types I~IV) based on $\tau(0.5)$ and α data observed at the three sites. We defined aerosols with smaller $\tau(0.5)$ than the total mean $\tau(0.5)$ and greater than or equal to the total mean of α ($\tau(0.5) < \bar{\tau}(0.5), \alpha \geq \bar{\alpha}$) as Type-I,

those with $\tau(0.5) \geq \bar{\tau}(0.5)$ and $\alpha \geq \bar{\alpha}$ as Type-II, those with $\tau(0.5) < \bar{\tau}(0.5)$ and $\alpha < \bar{\alpha}$ as Type-III, and those with $\tau(0.5) \geq \bar{\tau}(0.5)$, $\alpha < \bar{\alpha}$ as Type-IV. The most common aerosol is Type-I (~40%) at all three sites. Type-IV aerosols show the same seasonal cycle (spring maximum) at all three sites, suggesting that large-scale phenomena, such as Asian dust events, contribute to the production and transport of this aerosol type. The behavior of Type-II aerosols differs between the three sites, indicating that local phenomena most likely contribute to the production and transport of Type-II aerosols. Anthropogenic aerosol emission and the subsequent gas-to-particle processes likely contribute to the formation of Type-II aerosols. Type-III aerosols have a seasonal cycle of opposite phase to that of Type-IV at Sapporo, suggesting a difference in the sources and/or transport processes of larger particles between spring and autumn.

3. We compared atmospheric turbidity β retrieved from sky radiometer β(SR) with that calculated using direct solar radiation measurements β(DSR) at Sapporo. Although both turbidity measurements showed the same seasonal cycle, β(SR) was slightly smaller (~0.02) than β(DSR). To confirm these trends and to help explain the reason for the difference, we are continuing to monitor the aerosol optical properties using a sky radiometer.
4. Since the relative humidity is high under cloudy conditions, the optical properties of aerosols that exist between clouds can change. The sky radiometer can retrieve optical properties of aerosols even under cloudy conditions if there are no clouds around the solar aureole. It was found that the seasonal mean of $\tau(0.5)$ (or α) measured under cloudy conditions was 1.5 to 1.8 (1.1 to 1.2) times as large (small) as that measured under clear skies. In other words, the direct effect of aerosols that exist between clouds cannot be ignored. We called this the hybrid effect of aerosols.

Acknowledgments

We thank Prof. T. Nakajima (CCSR, Univ. of Tokyo), Prof. K. Kawamura, Dr. T. Endoh and Dr. M. Kawashima (ILTS, Hokkaido Univ.), Prof. K. Yamazaki and Dr. H. Hatsushika (Graduate School of Environmental Earth Science, Hokkaido Univ.), Prof. S. Ohta (Graduate School of Engineering, Hokkaido Univ.), Prof. K. Arao (Nagasaki Univ.) and Prof. E. Raschke (GKSS Research Center, Germany) for their useful comments and advices. We are also grateful to Drs. H. Nagata and T. Watanabe (Japan Sea National Fisheries Res. Inst.), Drs. N. Sugimoto, I. Matsui and A. Shimizu (National Inst. for Environ. Studies), Prof. M. Shiobara (National Inst. of Polar Res.), Prof. T. Murayama (Tokyo Univ. of Mercantile Marine) and Prof. T. Takamura (Center for SKYNET site of Chiba Univ.) for the data that they shared openly.

References

Ångström, A., 1961: Techniques of determining the turbidity of the atmosphere. *Tellus*, **13**, 214–223.

———, 1964: The parameters of atmospheric turbidity. *Tellus*, **16**, 64–75.

Arao, K., 1974: Recent change of atmospheric turbidity over Japan. *J. Meteor. Soc. Japan*, **52**, 506–508.

——— and K. Aoki, 2001: Yellow sand events in Springs 1999–2000 over Nagasaki, Japan. *J. Environmental Studies Nagasaki University*, **4**, 1–17 (in Japanese).

——— and Y. Ishizaka, 1986: Volume and mass of yellow sand dust in the air over Japan as estimated from atmospheric turbidity. *J. Meteor. Soc. Japan*, **64**, 79–94.

——— and H. Yamamoto, 1981: Atmospheric turbidity in 1970's and its secular variation over Japan. *Sci. Bull. Fac. Educ., Nagasaki University*, **32**, 87–98 (in Japanese).

Atmospheric Environment, 1981: *Special Issue on Arctic air chemistry*, **15**, 1345–1516.

———, 1985: *Special Issue on Arctic air chemistry*, **19**, 1987–2208.

———, 1989: *Special Issue on Arctic air chemistry*, **23**, 2345–2638.

Barrie, L.A., J.W. Bottenheim, R.C. Schnell, P.J. Crutzen and R.A. Rasmussen, 1988: Ozone destruction and photochemical reactions at polar sunrise in the lower Arctic atmosphere. *Nature*, **334**, 138–141.

Boi, P., G. Tonna, G. Dalu, T. Nakajima, B. Olivieri, A. Pompei, M. Campanilli and R. Rao, 1999: Calibration and data elaboration procedure for sky irradiance measurements. *Appl. Opt.*, **38**, 896–907.

Charlson, R.J., S.E. Schwartz, J.M. Hales, R.D. Cess, J.A. Coakley, Jr., J.E. Hansen and D.J. Hofmann, 1992: Climate forcing by anthropogenic aerosols. *Science*, **255**, 423–430.

Eck, T.F., B.N. Holben, D.E. Ward, O. Dubovik, J.S. Reid, A. Smirnov, M.M. Mukelabai, N.C. Hsu, N.T. O'Neill and I. Slutsker, 2001: Characterization of the optical properties of biomass burning aerosols in Zambia during the 1997 ZIBBEE field campaign. *J. Geophys. Res.*, **106**, 3425–3448.

Hayasaka, T., Y. Meguro, Y. Sasano and T. Takamura, 1998: Stratification and size distribution of aerosols retrieved from simultaneous measurements with lidar, a sunphotometer, and an aureolemeter. *Appl. Opt.*, **37**, 961–970.

Higurashi, A., T. Nakajima, B.N. Holben, A. Smirnov, R. Frouin and B. Chatenet, 2000: A study of global aerosol optical climatology with two-channel AVHRR remote sensing. *J. Climate*, **13**, 2011–2027.

Holben, B.N., T.F. Eck, I. Slutsker, D. Tanre, J.P. Buis, A. Setzer, E. Vermote, J.A. Reagan, Y.J. Kaufman, T. Nakajima, F. Lavenu, I. Jankowiak and A. Smirnov, 1998: AERONET—A federated instrument network and data archive for aerosol characterization. *Remote Sensing Environ.*, **66**, 1–16.

———, A. Setzer, T.F. Eck, A. Pereira and I. Slutsker, 1996: Effect of dry-season biomass burning on Amazon basin aerosol concentrations and optical properties, 1992–1994. *J. Geophys. Res.*, **101**, 19,465–19,481.

———, D. Tanre, A. Smirnov, T.F. Eck, I. Slutsker, N. Abuhassan, W.W. Newcomb, J.S. Schafer, B. Chatenet, F. Lavenu, Y.J. Kaufman, J.V. Castle, A. Setzer, B. Markham, D. Clark, R. Frouin, R. Halthore, A. Karneli, N.T. O'Neill, C. Pietras, R.T. Pinker, K. Voss and G. Zibordi, 2001: An emerging ground-based aerosol climatology: Aerosol optical depth from AERONET. *J. Geophys. Res.*, **106**, 12,067–12,097.

Husar, R.B., D.M. Tratt, B.A. Schichtel, S.R. Falke, F.L.D. Jaffe, S. Gasso, T. Gill, N.S. Laulainen, F. Lu, M.C. Reheis, Y. Chun, D. Westphal, B.N. Holben, C. Gueymard, I. McKendry, N. Kuring, G.C. Feldman, C. McClain, R.J. Frouin, J. Merrill, D. DuBois, F. Vignola, T. Murayama, S. Nickovic, W.E. Wilson, K. Sassen, N. Sugimoto and W.C. Malm, 2001: Asian dust events of April 1998. *J. Geophys. Res.*, **106**, 18,317–18,330.

Isono, K., K. Komabayashi and A. Ono, 1959: The nature and origin of ice nuclei in the atmosphere. *J. Meteor. Soc. Japan*, **37**, 211–233.

Jaffe, D.A., T. Anderson, D. Covert, R. Kotchenruther, B. Trost, J. Danielson, W. Simpson, T. Berntsen, S. Karlsdottir, D. Blake, J. Harris, G. Carmichael and I. Uno, 1999: Transport of Asian air pollution to North America. *Geophys. Res. Lett.*, **26**, 711–714.

Kaufman, Y.J., A. Setzer, D. Ward, D. Tanre, B.N. Holben, P. Menzel, M.C. Pereira and R. Rasmussen, 1992: Biomass burning airborne and spaceborne experiment in the Amazonas (BASE-A). *J. Geophys. Res.*, **97**, 14,581–14,599.

Kawamura, K., A. Yanase, T. Eguchi, T. Mikami and L.A. Barrie, 1996: Enhanced atmospheric transport of soil derived organic matter in spring over the high Arctic. *Geophys. Res. Lett.*, **23**, 3735–3738.

Liou, K.N., 1980: An introduction to atmospheric radiation, Academic. New York, p. 392.

Mizuno, T. and H. Kondo, 1992: Generation of a local front and high levels of air pollution on the Kanto Plain in early winter. *Atmospheric Environment*, **26A**, 137–143.

Murayama, T., N. Sugimoto, I. Uno, K. Kinoshita, K. Aoki, N. Hagiwara, Z. Liu, I. Matsui, T. Sakai, T. Shibata, K. Arao, B.J. Sohn, J.G. Won, S.C. Yoon, T. Li, J. Zhou, H. Hu, M. Abo, K. Iokibe, R. Koga and Y. Iwasaka, 2001: Ground-based network observation of Asian dust events of April 1998 in East Asia. *J. Geophys. Res.*, **106**, 18,345–18,360.

Nagoya University, 1991: Kosa. Kokin Syoin, Tokyo, 328pp (in Japanese).

Nakajima, T., A. Higurashi, K. Aoki, T. Endoh, H. Fukushima, M. Toratani, Y. Mitomi, B.G. Mitchell and R. Frouin, 1999a: Early phase analysis of OCTS radiance data for aerosol remote sensing. *IEEE Trans. Geosci. Remote Sensing*, **37**, 1575–1585.

———, ———, N. Takeuchi and J.R. Harman, 1999b: Satellite and ground-based study of optical properties of 1997 Indonesian forest fire aerosols. *Geophys. Res. Lett.*, **26**, 2421–2424.

——— and M. Tanaka, 1986: Matrix formulations for the transfer of solar radiation in a plane-parallel scattering atmosphere. *J. Quant. Spectrosc. Radiat. Transfer*, **35**, 13–21.

———, ——— and T. Yamauchi, 1983: Retrieval of the optical properties of aerosols from aureole and extinction data. *Appl. Opt.*, **22**, 2951–2959.

———, G. Tonna, R. Rao, P. Boi, Y. Kaufman and B. Holben, 1996: Use of sky brightness measurements from ground for remote sensing of particulate polydispersions, *Appl. Opt.*, **35**, 2672–2686.

Ohta, S., N. Murao, S. Yamagata, T. Fukasawa, S. Hasegawa and K. Arao, 1997: Variation in atmospheric turbidity in the area around Japan. *J. Global Environment Engineering*, **3**, 9–21.

Sassen, K. and B.S. Cho, 1992: Subvisual-thin cirrus lidar data set for satellite verification and climatological research. *J. Appl. Meteor.*, **31**, 1275–1285.

Shaw, G.E., 1979: Inversion of optical scattering and spectral extinction measurements to recover aerosol size spectra. *Appl. Opt.*, **18**, 988–993.

———, 1980: Transport of Asian dust aerosol to the Hawaiian islands. *J. Appl. Meteor.*, **19**, 1254–1259.

Shiobara, M., T. Hayasaka, T. Nakajima and M. Tanaka, 1991: Aerosol monitoring using a scanning spectral radiometer in Sendai, Japan. *J. Meteor. Soc. Japan*, **69**, 57–70.

———, J.D. Spinhirne, A. Uchiyama and S. Asano, 1996: Optical depth measurements of aerosol, cloud, and water vapor using sun photometer during FIRE cirrus IFO II. *J. Appl. Meteor.*, **35**, 36–46.

Smirnov, A., B.N. Holben, T.F. Eck, O. Dubovik and I. Slutsker, 2000: Cloud-screening and quality control algorithms for the AERONET database. *Remote Sens. Environ.*, **73(3)**, 337–349.

Suzuki, K., O. Uchino, M. Yoshida, K. Honda, M. Aono, F. Watanabe and T. Ootomo, 2001: Kosa (Yellow sand) events in April, 1998 and 1999 observed by sun photometers. *Tenki*, **48**, 317–322 (in Japanese).

Takemura, T., T. Nakajima, T. Nozawa and K. Aoki, 2001: Simulation of future aerosol distribution, radiative forcing, and long-range transport in East Asia. *J. Meteor. Soc. Japan*, **79**, 1139–1155.

———, H. Okamoto, Y. Maruyama, A. Numaguti, A. Higurashi and T. Nakajima, 2000: Global three-dimensional simulation of aerosol optical thickness distribution of various origins. *J. Geophys. Res.*, **105**, 17,853–17,873.

Tanaka, M., M. Shiobara, T. Nakajima, M. Yamano and K. Arao, 1989: Aerosol optical characteristics in the yellow sand events observed in May, 1982 at Nagasaki—Part I Observations. *J. Meteor. Soc. Japan*, **67**, 267–278.

———, T. Takamura and T. Nakajima, 1983: Refractive index and size distribution of aerosols as estimated from light scattering measurements. *J. Clim. Appl. Meteor.*, **22**, 1253–1261.

Tanimoto, H., Y. Kajii, J. Hirokawa and H. Akimoto, 2000: The atmospheric impact of boreal forest fires in far eastern Siberia on the seasonal variation of carbon monoxide: Observations at Rishiri, a northern remote island in Japan. *Geophys. Res. Lett.*, **27**, 4073–4076.

Tegen, I., A.A. Lacis and I. Fung, 1996: The influence on climate forcing of mineral aerosols from disturbed soils. *Nature*, **380**, 419–422.

Tonna, G., T. Nakajima and R. Rao, 1995: Aerosol features retrieved from solar aureole data: a simulation study concerning a turbid atmosphere. *Appl. Opt.*, **34**, 4486–4499.

Tratt, D.M., R.J. Frouin and D.L. Westphal, 2001: April 1998 Asian dust event: A southern California perspective. *J. Geophys. Res.*, **106**, 18,371–18,379.

Twomey, S.A., M. Piepgrass and T.L. Wolfe, 1984: An assessment of the impact of pollution on global cloud albedo. *Tellus*, **36**, 356–366.

Uematsu, M., R.A. Duce, J.M. Prospero, L. Chen, J.T. Merrill and R.L. McDonald, 1983: Transport of mineral aerosol from Asia over the North Pacific Ocean. *J. Geophys. Res.*, **88**, 5343–5352.

Uno, I., H. Amano, S. Emori, K. Kinoshita, I. Matsui and N. Sugimoto, 2001: Trans-Pacific yellow sand transport observed in April 1998: A numerical simulation. *J. Geophys. Res.*, **106**, 18,331–18,344.

Yamamoto, G. and M. Tanaka, 1969: Determination of aerosol size distribution from spectral attenuation measurements. *Appl. Opt.*, **8**, 447–453.

———, ——— and K. Arao, 1968: Hemispherical distribution of turbidity coefficient as estimated from direct solar radiation measurements. *J. Meteor. Soc. Japan*, **46**, 287–300.

———, ——— and ———, 1971: Secular variation of atmospheric turbidity over Japan. *J. Meteor. Soc. Japan*, **49**, 859–865.

Yamazaki, K., H. Yanagihara and K. Aoki, 1999: Simulation of generation and transport of Kosa aerosols, *Special Reports on the Regional Studies of North-East Eurasia and North Pacific in Hokkaido University*, Hokkaido University, 75–83.

Zhao, Y., Y. Kondo, F.J. Murcray, X. Liu, M. Koike, H. Irie, K. Strong, K. Suzuki, M. Sera and Y. Ikegami, 2000: Seasonal variation of HCN over northern Japan measured by ground-based infrared solar spectroscopy. *Geophys. Res. Lett.*, **27**, 2085–2088.